chroism in the magnetic peaks reverses sign for negative $\mathbf{q}_y$, as expected from symmetry arguments (*9*). Thus, instead of measuring with opposite light helicities, it would be sufficient to compare the magnetic peak intensities for just one spectrum but with opposite sign of $\mathbf{q}_y$.

To obtain more information about the magnetization depth profile, we measured CDXRMS spectra at different incidence angles. The results are shown in the inset of Fig. 2B, where the ratio of the difference intensity to the sum intensity, $I_A = (I^+ - I^-)/(I^+ + I^-)$, is plotted for the first- and second-order magnetic peaks. Following (*4*), we modeled the measured values taking into account all possible scattering channels according to Eq. 1 (*9*). The periodic lateral modulation of the magnetization was described by Fourier transforms. To simplify the analysis, we approximated the triangular closure domains by sine and cosine waves (Fig. 1C). From the specular reflectivity curve, we determined the x-ray absorption length in FePd at the Fe L_3 edge to be about 400 Å. For the grazing incidence angles used here, it is therefore sufficient to model the film as a semi-infinite slab, thus neglecting the bottom interface where closure domains can also occur.

The I_A signals for both magnetic satellite peaks show strong modulations with Θ. This is caused by a change in the phase relation between the signals from the closure and bulk domain layers as the wave vector perpendicular to the film is varied with Θ, and it provides a direct proof of the existence of closure domains with in-plane magnetization direction. Part of the I_A signals can also be attributed to interference between closure domains and domain walls with a magnetization direction perpendicular to the film within one layer (Fig. 1C); however, this contribution does not vary with Θ.

The amplitudes of the layer magnetization were deduced from modeling the first-order magnetic I_A signals (Fig. 1, C and D). These were representative of closure and bulk domains, respectively. Here, we assumed that the closure domains are distributed uniformly over an effective depth, t, from the surface of the film. The value of t is very sensitive to the angular position of the maxima and minima of $I_A(\Theta)$ in Fig. 2B. We obtain t = 125 Å. The factors $F_n^{(1)}$ in Eq. 1 are mainly proportional to the magnitude of the spin magnetic moment (*6*). Only the first-order Fourier coefficients shown in Fig. 1, C and D, contribute to the first-order magnetic peaks. However, both first-order and third-order Fourier coefficients are important for the second-order magnetic satellite peaks. This increased parameter set causes the fit to be overdetermined for the present limited data range, but this problem could be resolved by obtaining an extended data set in further measurements.

The second-order magnetic peaks are interesting because the factors $F_n^{(2)}$ in Eq. 1 contain contributions from other ground-state moments such as the anisotropic spin-orbit coupling. These quantities are of special importance in understanding the magnetocrystalline anisotropy (*15*).

References and Notes

1. P. Carra and B. T. Thole, *Rev. Mod. Phys.* **66**, 1509 (1994).
2. M. Blume, *J. Appl. Phys.* **57**, 3615 (1985).
3. D. Gibbs *et al.*, *Phys. Rev. Lett.* **61**, 1241 (1988).
4. J. P. Hill and D. F. McMorrow, *Acta Crystallogr.* **A52**, 236 (1996).
5. J. P. Hannon, G. T. Trammell, M. Blume, D. Gibbs, *Phys. Rev. Lett.* **61**, 1245 (1988).
6. J. Luo, G. T. Trammell, J. P. Hannon, *ibid.* **71**, 287 (1993).
7. J.-M. Tonnerre *et al.*, *ibid.* **75**, 740 (1995).
8. M. Sacchi *et al.*, *ibid.* **81**, 1521 (1998).
9. For more details, see Science Online (www.sciencemag.org/feature/data/990819.shl).
10. J. B. Kortright, T. M. Rice, R. Carr, *Phys. Rev. B* **51**, 10240 (1995).
11. C. Kao *et al.*, *Phys. Rev. Lett.* **65**, 373 (1990).
12. V. Gehanno, A. Marty, B. Gilles, Y. Samson, *Phys. Rev. B* **55**, 12552 (1997).
13. C. Kittel, *Phys. Rev.* **70**, 965 (1946).
14. C. Stamm *et al.*, *Science* **282**, 449 (1998).
15. G. van der Laan, *Phys. Rev. Lett.* **82**, 640 (1999).

16. We thank K. Larsson, O. Tjernberg, and N. B. Brookes for their help and technical assistance and the ESRF staff for the excellent operational conditions.

11 February 1999; accepted 27 April 1999

Homeotic Transformation of Rhombomere Identity After Localized *Hoxb1* Misexpression

Esther Bell, Richard J. T. Wingate, Andrew Lumsden*

Segmentation of the hindbrain and branchial region is a conserved feature of head development, involving the nested expression of *Hox* genes. Although it is presumed that vertebrate *Hox* genes function as segment identifiers, responsible for mediating registration between elements of diverse embryonic origin, this assumption has remained untested. To assess this, retroviral misexpression was combined with orthotopic grafting in chick embryos to generate a mismatch in *Hox* coding between a specific rhombomere and its corresponding branchial arch. Rhombomere-restricted misexpression of a single gene, *Hoxb1*, resulted in the homeotic transformation of the rhombomere, revealed by reorganization of motor axon projections.

Since the identification of homologs of *Drosophila* homeotic genes in vertebrates, a consensus model for their role during head development has emerged. The hindbrain is subdivided into rhombomeres, whereas adjacent tissues are subdivided into a series of branchial arches. Regional expression of *Hox* genes in the hindbrain is thought to confer identity to rhombomeres (*1*), whereas equivalent expression in the neural crest–derived branchial arches may provide a positional match between the two systems. Motor axons arising within a given pair of rhombomeres project to a single corresponding branchial arch (*2*). Targeted mutation (*3*–*5*), overexpression (*6*, *7*), or manipulation of *Hox* genes by exogenous retinoids (*8*) all support a *Hox* code model (*9*), but none of these approaches can specifically test the assumption that *Hox* genes act as segment identifiers mediating registration between structures along the anteroposterior axis of the head.

One way to address this issue is to gener-

Department of Developmental Neurobiology, King's College London, Guy's Hospital, London SE1 9RT, UK.

*To whom correspondence should be addressed. E-mail: andrew.lumsden@kcl.ac.uk

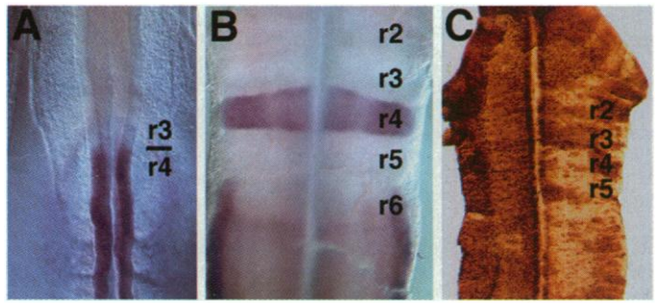

Fig. 1. Endogenous expression of *Hoxb1* at stages 9 (**A**) and 19 (**B**), and ectopic Hoxb1 expression (brown) in a stage 23 hindbrain after infection with RCAS/*Hoxb1* at stage 3 (**C**).

ate a mismatch of *Hox* gene expression between the hindbrain and periphery by confining overexpression to a specific domain. The expectation is that a homeotic transformation of the domain would be manifested by an orderly respecification of motor axon projections. Accordingly, we have compared the effects of globally overexpressing a single *Hox* gene, *Hoxb1*, with the effects of restricting its overexpression to a single rhombomere or branchial arch.

Hoxb1 has a rostral limit of expression at the boundary between rhombomere 3 (r3) and r4 (Fig. 1A) and is expressed at high levels in r4 throughout the period of overt segmentation (Fig. 1B) (*10*). Hoxb1 expression thus characterizes both facial motor neuron precursors in basal r4 (*4*) and the neural crest cells that migrate from dorsal r4 into facial motor neuron target regions of the second branchial arch (*11*). The gene is never expressed rostral to r4 or in the first branchial arch. To overexpress *Hoxb1* in chick embryos, we cloned the mouse gene into RCAS and RCAN retroviral vectors and used these to infect embryos (*12*) at Hamburger and Hamilton (*13*) stages 3 through 8. We analyzed embryos at stages 18 through 23, monitoring mouse Hoxb1 expression independently of endogenous *Hoxb1* (Fig. 1C).

In normal and control (RCAN/*Hoxb1*-infected) embryos, r4 can be distinguished from r2 both by molecular markers and by

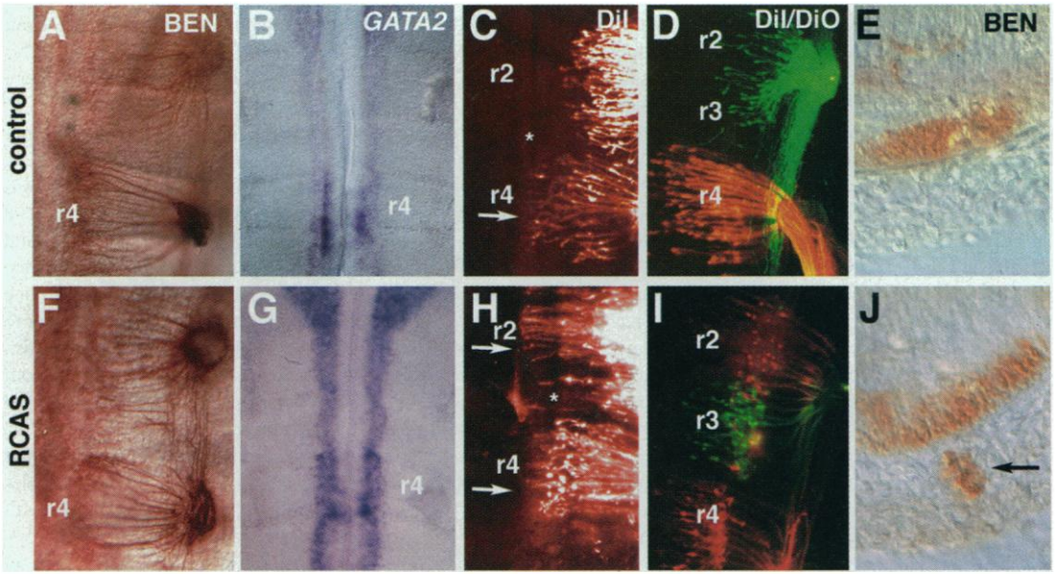

Fig. 2. Comparison of controls (**A** to **E**) and RCAS/*Hoxb1*-infected embryos (**F** to **J**). (A and F) BEN expression. (B and G) *GATA2* expression. (C and H) CVA neurons labeled with DiI (arrows; floor plate shown by asterisk). (D and I) Motor axon projections, revealed by retrograde tracing from first (green) and second (red) branchial arches. (E and J) BEN-stained hindbrains in transverse section, showing ectopic nerve (arrow).

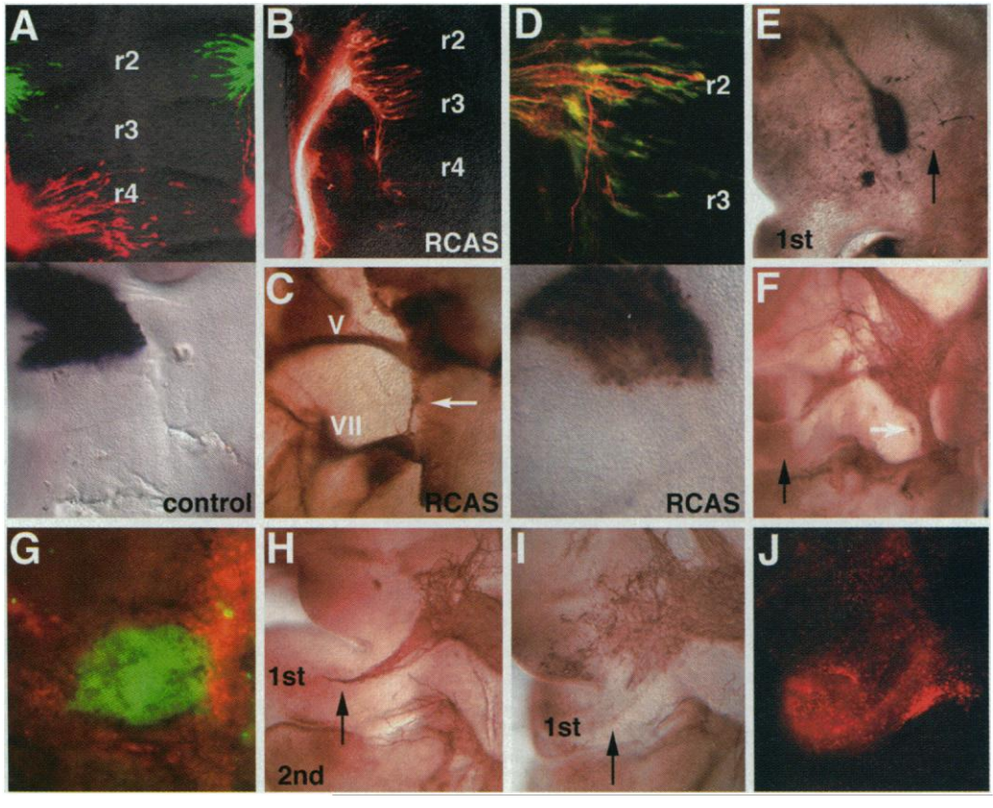

Fig. 3. Comparison of control (**A**) and RCAS/*Hoxb1*-infected (**B** to **D**) r2 basal plate orthotopic grafts. (A and D) Motor neurons traced from first (green) and second (red) arches (upper panels) and viral infection in the same grafts (lower panels). (B and C) Abnormal longitudinal fascicle of axons between r2 and the second arch, revealed by retrograde tracing (B) and in antibody to neurofilament (C) (arrow). (**E** to **G**) Failure of trigeminal motor neurons correctly to innervate first branchial arch territory ectopically expressing Hoxb1. (E) Unattached trigeminal ganglion, lacking motor nerve (arrow). (F) Fused trigeminal and facial ganglia (white arrow), truncated mandibular nerve (black arrow). (G) Uninfected graft (green) within Hoxb1-positive tissue (red). (**H** to **J**) Unilateral orthotopic graft of RCAS/*Hoxb1*-infected r2 alar plate into an uninfected embryo. Compare the normal appearance of the trigeminal ganglion and mandibular nerve (arrow) contralateral to the graft (H), with dispersion of the ganglion and truncation of the nerve (arrow) on the operated side (I), where first arch neural crest cells express Hoxb1 (J). V: trigeminal ganglion; VII: facial ganglion.

motor neuron migration behavior (Fig. 2, A to D). First, expression of the immunoglobulin (Ig) superfamily cell surface glycoprotein BEN (*14*) is substantially stronger in the (facial) motor neurons of r4 than in the (trigeminal) motor neurons of r2 (*15*) (Fig. 2A). Second, the transcriptional control gene *GATA2*, a putative downstream target of *Hoxb1* in motor neurons (*16*), is expressed transiently at higher levels in r4 than in r2 (Fig. 2B) (*17*). Third, an r4-specific population of contralaterally migrating (vestibuloacoustic) efferent (CVA) neurons (*18*) can be revealed by retrograde tracing (Fig. 2C) from the cranial nerve exit point in r4 (*19*). Fourth, retrograde labeling of motor neurons from the branchial arches reveals that r2 motor axons innervate the first arch and r4 motor axons innervate the second arch (*2*); this registration was observed in all uninfected embryos (n = 39) (*20*) and controls (n = 23) (Fig. 2D).

After global overexpression of Hoxb1, both BEN (Fig. 2F) and *GATA2* (Fig. 2G) are upregulated in r2, to levels normally seen in r4 (Fig. 2, A and B) (*10*). Retrograde labeling reveals extensive contralateral neuronal migration in r2 (n = 21) (Fig. 2H), suggesting the ectopic differentiation of CVA neurons. In the large majority of embryos (n = 32/35), the registration between motor nerves and their peripheral targets was unaltered, consistent with previous studies (*4*, *7*) in which *Hox* gene expression was changed globally. However, in a few RCAS/*Hoxb1*-infected embryos (n = 3/35), we noted a prominent reordering of motor axon trajectories. In these, r2 motor neurons were labeled not from their normal target, the first branchial arch, but from the second branchial arch (Fig. 2I), which they reached by way of an ectopic axon fascicle coursing longitudinally outside the hindbrain (Fig. 2, compare E and J). Thus, global overexpression of Hoxb1 can result in the transformation of r2 to r4, on the basis of molecular markers and motor neuronal migration, but rerouting of the ectopic "r4"-type motor neurons to the second arch is rare. The acquisition of a "normal" pattern of peripheral innervation may result from the transformed neurons still recognizing the first arch as an appropriate target because, with global overexpression, it too would have been transformed to a more posterior identity. The occasional rerouting of "r4"-type motor axons is consistent with this possibility, if it is assumed that the mosaic nature of infection happened to spare the first arch. This, in turn, suggests that rerouting would be a predictable consequence of confining overexpression to the basal plate of the neural tube.

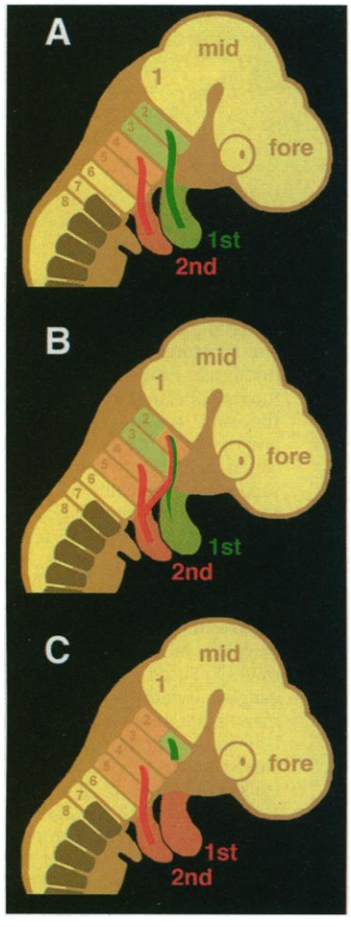

Fig. 4. Summary diagrams showing the registration between hindbrain (r2 and r4) and branchial arches (1st and 2nd) in normal embryos (**A**), and when Hoxb1 expression is targeted to the basal plate of r2 (**B**) or first arch tissues (**C**).

Thus, we explanted the r2 basal plate of stage 10 through 11 embryos that had been globally infected at stage 3 with RCAS(N)/*Hoxb1* and grafted these orthotopically into stage-matched, virus-resistant hosts (n = 22). Orthotopic grafting was as described (*21*), and embryos were harvested at stage 19 through 20. As expected for controls, motor neurons arising in r2 grafts that were infected with the RCAN/*Hoxb1* virus (n = 5), or were uninfected (n = 14), always sent their axons exclusively to the first branchial arch (Fig. 3A, upper panel). By contrast, where the grafted basal r2 showed high levels of Hoxb1 expression, we found that motor neurons projected aberrantly to the second branchial arch at a high frequency (n = 12/17) (Fig. 3, B to D). Both carbocyanine dye tracing (n = 7/9) (Fig. 3B) and whole antibody to neurofilament staining (n = 5/8) (Fig. 3C) revealed a prominent ectopic nerve between the exit point in r2 and the root of the second arch. In all cases, there was no *Hoxb1* expression outside the graft (Fig. 3, A and D, lower panels). Neighboring motor neurons within RCAS/*Hoxb1*-infected basal r2 grafts sometimes projected to different branchial arches (Fig. 3D, upper panel). This would be consistent with a cell-autonomous effect of Hoxb1 on the choice of cell identity, if it could be shown to correlate with mosaicism of infection.

To test the extent to which *Hoxb1*-infected basal r2 replicates the normal r4 phenotype, we also grafted uninfected r4 basal plates heterotopically into the r2 basal plate position. Motor neurons from the graft (n = 7/8) (*20*) behaved identically to r2 motor neurons expressing Hoxb1 (Fig. 3B).

Finally, we performed a complementary series of grafts to examine the effects of *Hox* gene misexpression in the target, independent of the basal plate of the neural tube, where motor neurons are born. Two grafting strategies were used, with motor axon outgrowth assessed by neurofilament staining. First, grafts of quail basal r2 were transplanted, unilaterally and orthotopically, into chick embryos that were heavily infected with RCAS/*Hoxb1* (n = 7). In some embryos, no motor axons could be observed exiting the hindbrain (n = 3) (Fig. 3E), whereas in others, first arch innervation was extensively disrupted and trigeminal and facial ganglia were fused (n = 4) (Fig. 3F). No viral spread from host to donor tissue was detected (Fig. 3G), and effects were confined to the operated side of the embryo. Second, in order to target gene manipulation to neural crest derivatives in the first arch, r2 alar plates from RCAS/*Hoxb1*-expressing embryos (infected at stage 3) were transplanted, unilaterally and orthotopically, into virus-resistant host embryos at stage 8. By stages 18 through 21, crest derivatives expressing Hoxb1 colocalized with disruptions in trigeminal ganglion morphology (n = 4/5). Although development was normal on the control side of the embryo (contralateral to the graft) (Fig. 3H), the mandibular (motor component of the trigeminal) nerve was truncated (Fig. 3I) in the region of ectopic Hoxb1 expression (Fig. 3J).

By surgically restricting ectopic Hoxb1 expression to the basal plate of a rhombomere that lies anterior to the limit of endogenous expression, we have demonstrated a reassignment of motor neuron identity (Fig. 4B), as assessed by axonal trajectory. Using complementary grafting strategies, we have also shown that normal axon projections into the periphery are truncated when the target selectively expresses an inappropriate *Hox* gene (Fig. 4C).

These observations have implications for the interpretation of a number of previous studies where *Hox* gene levels were altered throughout the embryo. They also define precisely the previously uncertain role of *Hox* genes in coordinating segmental aspects of head development (*22*). First, the contrast between the effects of global and targeted misexpression explains the lack of systematic axonal respecification after global, targeted mutation of *Hox* genes in mice (*4*, *7*). Second, *Hox* genes appear to mediate appropriate connectivity between neural tube and peripheral targets by regulating a system of recognition cues shared by both tissues. By target-

ing gene misexpression to one rhombomere, the registration between neural tube and branchial arches can be systematically disrupted, overriding the normal segregation of branchiomeric segments. These results demonstrate that a classical homeotic transformation (*23*), in terms of gene expression, neuronal migration, and axon targeting, can be induced in a defined neuronal population by the ectopic expression of a single *Hox* gene. Thus, in vertebrates, as in flies, the role of *Hox* genes is to confer positional identity on individual elements of a meristic series.

References and Notes

1. A. Lumsden and R. Krumlauf, *Science* **274**, 1109 (1996).
2. A. Lumsden and R. Keynes, *Nature* **337**, 424 (1989).
3. M. Gendron-Maguire, M. Mallo, M. Zhang, T. Gridley, *Cell* **75**, 1317 (1993); F. M. Rijli *et al.*, *ibid.*, p. 1333.
4. J. M. Goddard, M. Rossel, N. R. Manley, M. R. Capecchi, *Development* **122**, 3217 (1996); M. Studer, A. Lumsden, L. Ariza-McNaughton, A. Bradley, R. Krumlauf, *Nature* **384**, 630 (1996).
5. A. Gavalas, M. Davenne, A. Lumsden, P. Chambon, F. M. Rijli, *Development* **124**, 3693 (1997); M. Mark *et al.*, *ibid.* **119**, 319 (1993); E. M. Carpenter, J. M. Goddard, O. Chisaka, N. R. Manley, M. R. Capecchi, *ibid.* **118**, 1963 (1993); O. Chisaka, T. S. Musci, M. R. Capecchi, *Nature* **355**, 516 (1992); A. Gavalas *et al.*, *Development* **125**, 1123 (1998); L. Tiret, H. Le Mouellic, M. Maury, P. Brulet, *ibid.*, p. 279.
6. D. Alexandre *et al.*, *Development* **122**, 735 (1996); A. C. Burke and C. J. Tabin, *Dev. Biol.* **178**, 192 (1996).
7. M. Zhang *et al.*, *Development* **120**, 2431 (1994).
8. H. Marshall *et al.*, *Nature* **360**, 737 (1992); J. Hill, J. D. Clarke, N. Vargesson, T. Jowett, N. Holder, *Mech. Dev.* **50**, 3 (1995).
9. P. Hunt *et al.*, *Nature* **353**, 861 (1991).
10. Whole-mount RNA in situ hybridizations were performed according to established protocols [D. Henrique *et al.*, *Nature* **375**, 787 (1995)]. All embryos stained for BEN and *GATA2* were processed identically. Immunohistochemistry was performed with the BEN, QCPN (quail-specific marker; Hybridoma bank, IA), RMO-270 (recognizes the 155-kD neurofilament subunit; Zymed, CA), and antimouse Hoxb1 antibodies (M. Capecchi and N. Manley).
11. O. H. Sundin and G. A. Eichele, *Genes Dev.* **4**, 1267 (1990).
12. The full coding region of mouse *Hoxb1* was subcloned as an Nco I–Hind III fragment into the adapter plasmid pCla12Nco. A Hind III restriction site was added after the stop codon by polymerase chain reaction. All sequences were verified by dideoxynucleotide chain termination sequencing. The adapter plasmid was cut with Cla I and the resulting insert subcloned into the Cla I site of RCAS(BP)A, RCAN(BP)A, RCAS(BP)B, and RCAN(BP)B vectors [S. H. Hughes, J. J. Greenhouse, C. J. Petropoulos, P. Sutrave, *J. Virol.* **61**, 3004 (1987); J. Gilthorpe, unpublished data]. The RCAS vector is capable of producing Hoxb1 protein, whereas the control RCAN vector, which lacks a splice acceptor site immediately 5′ of *Hoxb1*, is unable to produce Hoxb1 protein. Infectious virions were concentrated and injected into chick embryos [RCAS(BP)B-susceptible Hi-Sex white] at stages 3 to 8 according to established protocols [B. M. Morgan and D. M. Fekete, in *Methods in Avian Embryology*, M. Bronner-Fraser, Ed. (Academic Press, San Diego, CA, 1996), vol. 51, pp. 186–217]. Titers ranged between 10^8 and 10^9 infectious viral particles per milliliter. Ectopic Hoxb1 protein was detected with a mouse-specific polyclonal antibody, and *Hoxb1* mRNA by in situ hybridization, with a species-specific RNA probe.
13. V. Hamburger and L. Hamilton, *J. Morphol.* **88**, 49 (1951).
14. O. Pourquié, M. Coltey, J.-L. Thomas, N. Le Douarin, *Development* **109**, 743 (1990).
15. S. Guthrie and A. Lumsden, *ibid.* **114**, 663 (1992).
16. I. Pata *et al.*, in preparation.
17. E. Bell, A. Lumsden, A. Graham, *Mech. Dev.*, in press.
18. H. Simon and A. Lumsden, *Neuron* **11**, 209 (1993).
19. Retrograde labeling of motor neurons was performed by injection of either DiI [Molecular Probes, OR; 6 mg/ml in dimethylformamide (DMF)] or DiO (Molecular Probes; 10 mg/ml in DMF) into the first or second branchial arch (or both). Embryos were stored in the dark at room temperature in 4% paraformaldehyde for 7 to 14 days. Hindbrains were dissected and examined by confocal microscopy (Bio-Rad MRC 600).
20. E. Bell, R. J. T. Wingate, A. Lumsden, data not shown.
21. R. J. T. Wingate and A. Lumsden, *Development* **122**, 2143 (1996).
22. M. Goulding [*Neuron* **21**, 943 (1998)] proposes a role for *Hox* genes in specifying the identity and pathfinding characteristics of motor neurons.
23. W. Bateson, *Materials for the Study of Variation* (Cambridge Univ. Press, Cambridge, 1894).

24. We are grateful to S. Hughes for the pCla12Nco, RCAS(BP)A, RCAN(BP)A, and RCAS(BP)B vectors; J. Gilthorpe for the RCAN(BP)B vector; and R. Krumlauf for the mouse *Hoxb1* cDNA. We thank V. Prince and A. Graham for the chick *Hoxb1* and *GATA2* in situ probes, respectively, and M. Capecchi and N. Manley for the mouse antibody to Hoxb1. The BEN and QCPN monoclonal antibodies developed by N. Le Douarin and O. Pourquié and B. Carlson and J. Carlson, respectively, were obtained from the Developmental Studies Bank maintained by the University of Iowa, Department of Biological Sciences, under contracts N01-HD-7-3263 from the National Institute of Child Health and Human Development. The Wellcome Trust and the Medical Research Council supported this work. R.J.T.W. is a recipient of a Wellcome Career Development Award.

8 February 1999; accepted 11 May 1999

Odor Response Properties of Rat Olfactory Receptor Neurons

P. Duchamp-Viret,* M. A. Chaput, A. Duchamp

Molecular biology studies of olfaction have identified a multigene family of molecular receptors that are likely to be involved in odor transduction mechanisms. However, because previous functional data on peripheral coding were mainly collected from inferior vertebrates, it has been difficult to document the degree of specificity of odor interaction mechanisms. As a matter of fact, studies of the functional expression of olfactory receptors have not demonstrated the low or high specificity of olfactory receptors. In this study, the selectivity of olfactory receptor neurons was investigated in the rat at the cellular level under physiological conditions by unitary extracellular recordings. Individual olfactory receptor neurons were broadly responsive to qualitatively distinct odor compounds. We conclude that peripheral coding is based on activated arrays of olfactory receptor cells with overlapping tuning profiles.

The molecular receptive range (*1*) of olfactory receptor neurons (ORNs) is defined by the specificity of their olfactory receptors (ORs) regarding the structure of odor molecules and by the number and diversity of ORs expressed by the same neuron. Evidence has been provided that ORNs can express only one receptor subtype (*2*), so that ORNs may have a narrowly tuned specificity (*3*, *4*). Furthermore, the expression of ORs has been shown to be spatially segregated, and such an organization was proposed as defining the chemotopy of the olfactory mucosa (*5*). The rules governing the projection of ORNs to the olfactory bulb apparently support the spatial ORNs' segregation (*6*, *7*). If one takes these assumptions and results literally, the qualitative discrimination of odor molecules follows the coding scheme of a "labeled line system" (*8*) that is an extreme version of the one ORN–one OR hypothesis (*2*). In contrast, if broad tuning is assigned to ORs (*7*), this hypothesis is consistent with functional data on the qualitative tuning of ORNs in vivo. However these data have been mainly collected in amphibians, where individual ORNs respond to structurally different odor molecules (*9*, *10*). One may envisage that there is a real gap between molecular data obtained in mammals and cellular data obtained in amphibians that may be ascribed to phylogenetic evolution, if one assumes that ORNs become more and more selective. Such an explanation is in disagreement with the broad responsivity of mammalian olfactory bulb mitral cells (*11*), and our knowledge of the response properties of individual ORNs in intact mammals is limited (*12*). Thus, the question of the range of the chemical receptive field of individual ORNs was addressed by means of classical extracellular recording techniques in anesthetized rats.

Individual ORNs were recorded in vivo in freely breathing (n = 19) or tracheotomized (n = 16) rats (*13*). Ninety ORNs were recorded, generally in the endoturbinate II, during periods ranging from 20 min to 2 hours. The electro-olfactogram (EOG) was simultaneously recorded as close as possible to the single-unit record-

Laboratoire de Neurosciences et Systèmes Sensoriels, CNRS, UMR, Université Claude Bernard, 43 boulevard du 11 novembre 1918, 69622 Villeurbanne cedex, France.

*To whom correspondence should be addressed. E-mail: pduchamp@olfac.univ-lyon1.fr